Table 2
X-ray data-collection statistics.

Values in parentheses refer to the highest resolution shell, 2.85–2.75 Å.

Space group	*C*2
Unit-cell parameters	
a (Å)	145.9
b (Å)	52.3
c (Å)	169.0
β (°)	101.8
Resolution (Å)	20–2.75
Observed reflections	96908
Unique reflections	32335 (2865)
R_{merge}† (%)	6.7 (16.2)
Completeness (%)	98.3 (89.2)
$I/\sigma(I)$	12.7 (5.2)
Average redundancy	3.0 (1.8)

† $R_{merge} = (\sum|I_i - \langle I\rangle|/\sum I_i)/100$, where I_i is an individual intensity observation, $\langle I\rangle$ is the mean intensity for that reflection and the summation is over all reflections.

calculated to be 2.036 $Å^3\,Da^{-1}$ assuming two molecules (MW = 37 000 Da) of SDH to be present in the asymmetric unit (the remaining two molecules of the tetramer may be generated by crystallographic symmetry) and the estimated solvent content was 39.7% (Matthews, 1968).

Following the methodology described in the structure determination of rat SDH (Johansson *et al.*, 2001), the molecular-replacement method utilizing the coordinates of *C. beijerinckii* ADH (PDB code 1ped) as the starting model is currently being applied to solve the crystal structure of human SDH (atomic coordinates for rat SDH have yet to be deposited in the PDB). There is 22% sequence identity between *C. beijerinckii* ADH and human SDH. This will be the first crystal structure determined for human SDH. The structure will help to elucidate the catalytic mechanism and accurately model the interactions of the enzyme with substrate and inhibitor. Additionally, the comparisons between the crystal structures of human SDH, rat SDH and mammalian alcohol dehydrogenase will reveal important information about the different structural features between their active sites that are responsible for the differences in their substrate and inhibitor specificities. This information may be useful in the development of specific drugs for the treatment of diabetic complications.

References

Barretto, O. C., Nomoyama, K., Federsoni, P., Fedullo, J. D. & Diniz, L. B. (1985). *Comput. Biochem. Physiol. B*, **82**, 317–319.

Bradford, M. M. (1976). *Anal. Biochem.* **72**, 248–254.

Darmanin, C. & El-Kabbani, O. (2001). *Bioorg. Med. Chem. Lett.* **11**, 3133–3136.

Eklund, H., Horjales, E., Jörnvall, H., Brändén, C. & Jeffery, J. (1985). *Biochemistry*, **24**, 8005–8012.

Höög, J.-O., Karlsson, C., Eklund, H., Shapiro, R. & Jörnvall, H. (1993). *Adv. Exp. Med. Biol.* **328**, 439–450.

Hurley, T. D., Bosron, W. F., Hamilton, J. A. & Amzel, L. M. (1991). *Proc. Natl Acad. Sci. USA*, **88**, 8149–8153.

Iwata, T., Popescu, N. C., Zimonjic, D. B., Karlsson, C., Höög, J.-O., Vaca, G., Rodriguez, I. R. & Carper, D. (1995). *Genomics*, **26**, 55–62.

Jedziniak, J. A., Chylack, L. T., Cheng, H.-M., Gillis, M. K., Kalustian, A. A. & Tung, W. H. (1981). *Invest. Ophthalmol. Visual Sci.* **20**, 314–326.

Jeffery, J., Chesters, J., Millis, C., Sadler, P. J. & Jörnvall, H. (1984). *EMBO J.* **3**, 357–360.

Jeffery, J., Cummins, L., Carlquist, M. & Jörnvall, H. (1981). *Eur. J. Biochem.* **120**, 229–234.

Johansson, K., El-Ahmad, M., Kaiser, C., Jörnvall, H., Eklund, H., Höög, J.-O. & Ramaswamy, S. (2001). *Chem. Biol. Interact.* **130–132**, 351–358.

Kinoshita, J. H. & Nishimura, C. (1998). *Diabetes Metab. Res.* **4**, 323–337.

Korkhin, Y., Kalb, A. J., Peretz, M., Bogin, O., Burstein, Y. & Frolow, F. (1998). *J. Mol. Biol.* **278**, 967–981.

McPherson, A. (1985). *Methods Enzymol.* **114**, 112–125.

Maret, W. & Auld, D. S. (1988). *Biochemistry*, **27**, 1622–1628.

Matthews, B. W. (1968). *J. Mol. Biol.* **33**, 491–497.

O'Brien, M. M., Schofield, P. J. & Edwards, M. R. (1983). *Biochem. J.* **211**, 81–90.

Obrosova, I., Fathallah, L. & Lang, H.-J. (1999). *Biochem. Pharmacol.* **54**, 1945–1954.

Otwinowski, Z. & Minor, W. (1997). *Methods Enzymol.* **276**, 307–326.

The Diabetes Control and Complication Trials Group (1993). *New Engl. J. Med.* **7**, 843.

Exp. Anim. 52(2), 129–135, 2003

Molecular Cloning of ELOVL4 Gene from Cynomolgus Monkey (Macaca fascicularis)

Shinsuke UMEDA[1, 2], Radha AYYAGARI[3], Michihiro T. SUZUKI[4], Fumiko ONO[4], Fumino IWATA[5], Keiko FUJIKI[5], Atsushi KANAI[6], Yuichiro TAKADA[3], Yasuhiro YOSHIKAWA[2], Yasuhiko TANAKA[1], and Takeshi IWATA[1]

[1]National Institute of Sensory Organs, National Tokyo Medical Center, 2-5-1 Higashigaoka, Meguro-ku, Tokyo 152-8902, [2]Department of Biomedical Science, Graduate School of Agricultural and Life Sciences, The University of Tokyo, 1-1-1 Yayoi, Bunkyo-ku, Tokyo 113-8657, Japan, [3]Department of Ophthalmology, Kellogg Eye Center, University of Michigan, 1000 Wall Street, Ann Arbor, MI 48105, U.S.A., [4]The Corporation for Production and Research of Laboratory Primates, 1 Hachimandai, Tsukuba-shi, Ibaraki 305-0843, [5]Department of Ophthalmology, Juntendo University School of Medicine, 3–1–3 Hongo, Bunkyo-ku, Tokyo 113-8431, and [6]Department of Ophthalmology, Tokyo Metropolitan Koto Geriatric Medical Center, Tokyo 136-0075, Japan

Abstract: *ELOVL4, elongation factor of very long chain fatty acids-4, is known to be responsible for autosomal dominant macular degeneration and Stargardt-like macular degeneration. In this study, we cloned the monkey homologue of ELOVL4 and determined the cellular and tissue distribution of the gene product. Sequence analysis of the monkey ELOVL4 gene revealed a high degree of homology between human and monkey. The cloned full-length cDNA of monkey ELOVL4 encoded 314 amino acids, the same length as human and two amino acids longer than mouse. The monkey ELOVL4 conserved the characteristics typical of the super family of ELO enzymes involved in the metabolism of membrane-bound fatty acid elongation. Real-time quantitative PCR demonstrated that the monkey ELOVL4 gene was highly expressed in restricted tissue-specific fashion, not only in the retina but also in the skin (90% of retina) and thymus (111% of retina). Immunohistochemical analysis detected signals predominantly in the photoreceptor layer of the monkey retina.*

Key words: *cynomolgus monkey, ELOVL4, fatty acid, macular degeneration, photoreceptor metabolism*

Introduction

Stargardt-like macular dystrophy (STGD3) and autosomal dominant macular dystrophy (adMD) are inherited forms of macular degeneration characterized by decreased visual acuity, central macular atrophy and extensive fundus flecks, resulting in loss of central vision between 5 and 23 years of age [1–4]. The disease locus for adMD/STGD3 was localized to 6q14 by linkage analysis [4]. A novel gene, an elongation factor of

(Received 8 November 2002 / Accepted 24 December 2002)

Address corresponding: T. Iwata, National Institute of Sensory Organs, National Tokyo Medical Center, 2–5–1 Higashigaoka, Meguro-ku, Tokyo 152-8902, Japan

very long chain fatty acids-4 (*ELOVL4*), encoding a protein of 314 amino acids and homologous to the ELO gene family, was found to be associated with adMD/STGD3. The human *ELOVL4* gene is composed of 6 exons, and a 5 bp deletion in exon 6 that resulted in frame shift and the truncation of the protein was found in patients with adMD/STGD3 [5]. In addition, two 1-bp deletions separated by four nucleotides were detected in a family with macular dystrophy [6].

The *ELOVL4* gene is the fourth gene to be included in the *ELO* family which is involved in the membrane-bound fatty acid elongation system [7]. *ELO1 (Ssc1)* is required for microsomal fatty acid chain elongation between C14 and C16 [8]. *ELO2 (Ssc2)*, *ELO3 (Cig30)*, and other members of the *ELO* gene family are necessary for producing 26-carbon, very long chain fatty acids (VLCFA), which become precursors for ceramide and sphingolipids [9, 10]. *ELO1* is ubiquitously expressed in major tissues, while *ELO2* and *ELO3* show restricted tissue-specific expression [10]. The human *ELOVL4* gene is expressed in the brain, testis and specifically in the photoreceptor layer of the retina. Northern blot analysis showed the presence of a 2.9 kb transcript of *ELOVL4* mRNA in the brain, testis and retina where it was found abundantly. *In situ* hybridization of rhesus monkey and mouse retinal sections demonstrated that *ELOVL4* is expressed exclusively in photoreceptor cells [5]. However, in other major tissues, the expression levels of the *ELOVL4* gene have not yet been thoroughly examined.

Macula is found only in primates and birds, and the animal model for macular degeneration is currently limited to monkeys [11–14]. Thus the monkey model is extremely important for understanding the mechanisms and etiology underlying macular degenerative diseases in humans [15, 16]. We have reported a monkey model, which manifested early onset macular degeneration [17, 18]. The cynomolgus monkeys (*Macaca fascicularis*) show signs, such as drusen in the macula and lipofuscin deposit in the retinal pigment epithelium (RPE), consistent with the phenotype observed in age-related macular degeneration in humans. The pattern of inheritance is autosomal dominance.

Monkey homologs of genes responsible for macular degeneration in humans will serve as good candidates for the hereditary macular degeneration in these cynomolgus monkeys. In this study, we describe cloning and characterization of the monkey *ELOVL4* gene and its expression in various tissues.

Materials and Methods

Animal and Tissue Collection

All experimental procedures including maintenance and care of monkeys were conducted in accordance with the Guidelines for Animal Experimentation established by the Japanese Association for Laboratory Animal Science (1987). Eyes and other tissues of cynomolgus monkeys (*Macaca fascicularis*) including heart, liver, pancreas, ileum, kidney, thymus, spleen, lymph node, skin, skeleton muscle, cerebrum and cerebellum were obtained from Tsukuba Primate Center for Medical Science, National Institute of Infectious Diseases. These tissues were collected from the age group between 4–6 years, and stored for 1 day at 4°C in RNA stabilization solution (RNAlater, Ambion, Austin, TX) until RNA extraction.

Extraction of Genomic DNA and Total RNA

Genomic DNA was prepared from minced sclera using a DNA Extraction Kit (QIAamp DNA Mini Kit, QIAGEN, Valencia, CA) and total RNA was extracted using a RNA extraction reagent (TRIzol, Invitrogen, Carlsbad, CA) as directed by the manufacturer.

Analysis of the Monkey ELOVL4 *Gene Structure*

PCR of monkey genomic DNA using gene-specific primers (Table 1) and LA-Taq polymerase (TAKARA, Ohtsu, Japan) was performed. Primers were designed according to the human genomic DNA sequence submitted in a public database (GenBank accession number NT_017020). Amplified products were sequenced directly, or after being subcloned into pCRII cloning vector (TA Cloning Kit Dual Promoter, Invitrogen, Carlsbad, CA) using CEQ2000XL DNA analysis system and dye terminator sequencing kit (Beckman Coulter, Fullerton, CA). The 5'/3'-rapid amplification of cDNA ends (5'/3'-RACE) was performed using total RNA isolated from monkey retina and RPE. Primers were designed based on the obtained exon sequence in such a way that both 5'- and 3'-RACE products overlapped to cover full length cDNA. The primers used in this experiment were 5'-AATGAGCACTAGACGCATCTGA-3' and 5'-ATGCAGTCTCCTTGGCCTAC-3' for 5'-RACE

Table 1. Primer sets for analysis of *ELOVL4* gene structure

Forward primer			Reverse primer			Product
No.		Position	No.		Position	Size (kb)
P1	GGGTAGTGTCCTAAACGTAGTGTC	Exon 1	P2	ATCCCAGAGGCTTCAAGGA	Intron	4.5
P3	AACATCACCAGCTGGTAACATG	Intron	P4	AATGCTGCCAATGAACTCAA	Intron	4.7
P5	ATGCGATATTTAGCCTGAGAAGA	Intron	P6	ACTCTGAGGACAGTTGAAGATGAG	Intron	4.4
P7	AGAGAATAGGCTGCAGCAGAA	Intron	P8	ATCATGGAAGCTACAGTAACTGTCA	Intron	4.2
P9	ATTTGCATCTCATCAGAAGCAC	Intron	P10	AATGAGCACTAGACGCATCTGA	Exon 2	4.3
P11	ATGCAGTCTCCTTGGCCTAC	Exon 2	P12	ACATCGTACAGTGATGATACACATG	Exon 4	4.7
P13	ATAGCTGCTGCTCTGTGGTG	Exon 4	P14	AGTTGCAACATAGTCAGGTATCG	Exon 5	2.4
P15	AGCCCAGTTGAATTCCTTTATC	Exon 5	P16	AGGTAGCAGGGAATGAATAGCT	Exon 6	4.7

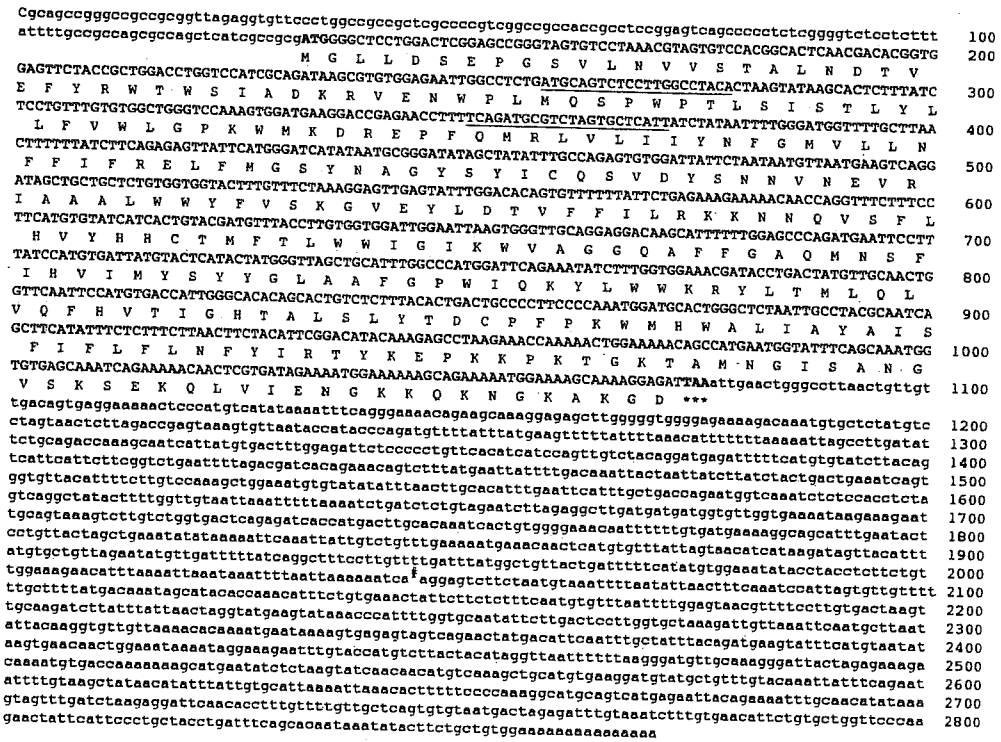

Fig. 1. Nucleotide sequence and encoded amino acid sequence of full-length monkey *ELOVL4* cDNA. The nucleotide sequence from the transcription initiation site to the poly(A) tail, encoding 314 amino acids, were determined by 5'- and 3'-RACE. Primers are also indicated (underlined). The numbering to the right refers to nucleotides and the capital single-letter below represents the corresponding amino acid. Asterisks and pound indicate stop codon and polyadenylation variant, respectively.

and 3'-RACE, respectively (Fig. 1). All procedures were carried out following the manufacturer's protocols (Invitrogen). Amplified PCR products were sequenced as described above.

Real-time Quantitative PCR

Total RNA from tissues was used to make cDNA with a first-strand synthesis system for RT-PCR (Superscript II, Invitrogen) as described by the manufacturer. In order to evaluate expression level in each tissue, we carried out real-time quantitative PCR with an ABI5700 system and SYBR Green reagent (PE Applied Biosystems, Foster, CA). The expression level was standardized with *GAPDH* as an internal control.

Table 2. The gene structure of monkey *ELOVL4*

Intron		Exon		Length	Intron		Approx. size
	CGCAGCCGGG ·····	1:	100 bp	TCCATCGCAG	gtaaagccgc ·····		20 kb
····· ttctctatag	ATAAGCGTGT ·····	2:	188 bp	····· CTTCAGAGAG	gtatgttttt ·····		1kb
····· ctttttccag	TTATTCATGG ·····	3:	81 bp	····· TGAAGTCAGG	gtaagtacat ·····		3 kb
····· ctttttacag	ATAGCTGCTG ·····	4:	172 bp	····· GGAGGACAAG	gtgagcattt ·····		2 kb
····· ttttctaaag	CATTTTTTGG ·····	5:	128 bp	····· GTTGCAACTG	gtgagttaaa ·····		2.5 kb
····· tgtttttcag	GTTCAATTCC ·····	6:	276 bp	····· TCTGCTGTGG			

Exon-intron organization of the monkey *ELOVL4* gene is shown. Ten nucleotides on both sides from the exon-intron boundaries are indicated. Open reading frame (ORF) length and approximate intron size are also indicated.

The primers P14 and P15 used for *ELOVL4* are shown in Table 1, and for *GAPDH*, forward primer 5'-CAGCCTCAAGATCATCAGCAAT-3', and reverse primer 5'-GGTCATGAGTCCTTCCACGATAC-3' were used. The PCR products were directly sequenced in order to confirm that the target cDNAs were precisely amplified.

Immunohistochemical Study for ELOVL4

Antibodies were raised by immunizing rabbits with peptide containing residues between 31 and 46 amino acids of human ELOVL4. Antiserum was used for immunohistochemistry on aldehyde-fixed frozen sections of monkey retina. In these experiments, preimmune serum was used for negative control.

Results

Sequence Analysis of the Monkey ELOVL4 *Gene*

Sequence analysis revealed that monkey *ELOVL4* cDNA and gene structures are very similar to those of humans (Table 2). The complete cDNA sequence of the monkey *ELOVL4* gene was 2,856 bp in length. The result from 3'-RACE indicated that an alternative splicing variant existed. This variant was 813 bp shorter and polyadenylated at the 3' non-coding region of exon 6 (Fig. 1).

The cDNA included 945 bp of open reading frame encoding 314 amino acids, the same length as human cDNA, and two amino acids longer than the mouse homologue (Fig. 2). There was a seven amino acid difference between monkey and human ELOVL4, but the monkey ELOVL4 also conserved features typical for members of the *ELO* gene family: a HXXHH motif

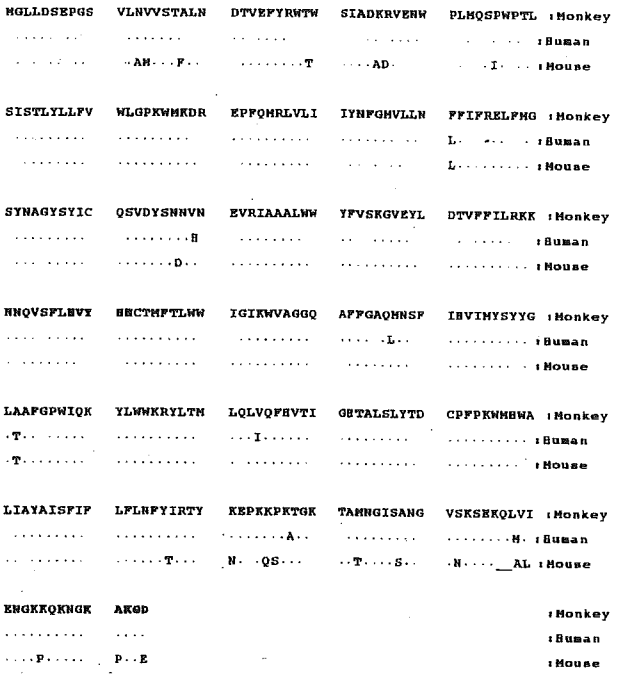

Fig. 2. Comparison of monkey amino acid sequence of *ELOVL4* protein with human and mouse. Monkey *ELOVL4* protein has a seven residue difference from human *ELOVL4* protein and is two residues longer than the mouse homologue. Dioxy iron-binding HXXHH motif and the carboxy-terminal dilysine signal, responsible for retention in endoplasmic reticulum, are also present in the monkey *ELOVL4* protein (shown bold).

identified in fatty acid desaturase and other dioxy iron cluster proteins [19]; and a KXKXX motif shown to be a strong signal for the retention of proteins in endoplasmic reticulum [20], where VLCFA are synthesized (Fig. 2) [21].

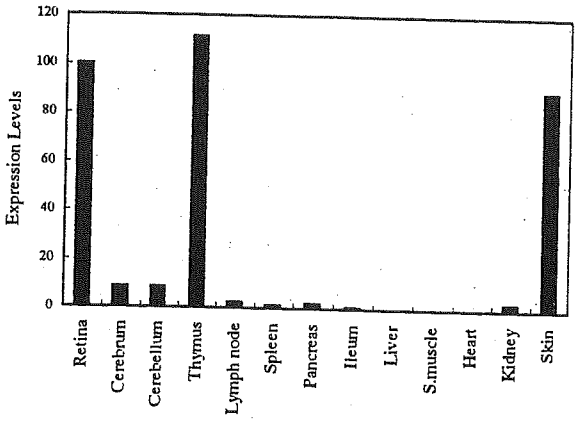

Fig. 3. Real-time quantitative PCR demonstrating tissue-restricted expression of *ELOVL4*. Abundant expression was observed not only in the retina but also in the thymus and skin at the same expression level. Expression level for each tissue is shown as a relative ratio compared to the retina.

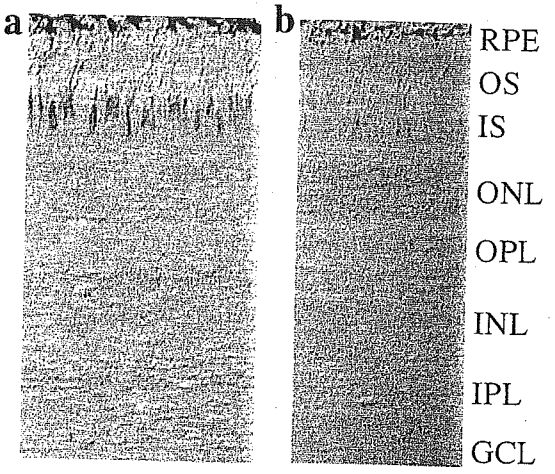

Fig. 4. Immunohistochemical analysis of monkey retina. a. Predominant signal is detected in the photoreceptor layer. b. Control hybridized with pre-immune serum, showing no signal. RPE, retinal pigment epithelium; OS, outer segments of photoreceptors; IS, inner segments of photoreceptors; ONL, outer nuclear layer; OPL, outer plexiform layer; INL, inner nuclear layer; IPL, inner plexiform layer; GCL, ganglion cell layer.

Expression of the Monkey ELOVL4 *Gene in Various Tissues*

Real-time quantitative PCR was performed on cDNA synthesized from total RNA from monkey retina, heart, liver, pancreas, ileum, kidney, thymus, spleen, lymph node, skin, skeletal muscle, cerebrum and cerebellum. The expression level in each tissue was calculated based on the standard curve created by PCR using a diluted plasmid containing *ELOVL4* cDNA fragment. The calculated values were evaluated after standardization with the expression level of *GAPDH* obtained in the same way.

The highest level of the *ELOVL4* gene expression was observed in the retina. Remarkable expressions were also detected in the thymus and skin. The expression levels in the thymus and skin were 111% and 90% of that in the retina, respectively. On the other hand, expression in the brain was shown to be less than 9% of that in the retina. In the other tissues, very low expression levels, just under 3% of that in the retina, were observed. In particular, in the liver and skeletal muscles, expression of the *ELOVL4* gene could not be detected (Fig. 3).

ELOVL4 *Expression in Monkey Retina*

Immunohistochemical analysis of monkey retinal sections showed prominent staining in photoreceptor inner segments (Fig. 4). These results are consistent with the observations made on the localization of the *ELOVL4* expression using *in situ* hybridization [5]. The presence of ELOVL4 was detected in both rod and cone photoreceptor cells.

Discussion

In this study, the genomic sequence and complete cDNA of the monkey *ELOVL4* gene, the fourth known homologue of the *ELO* gene family which encode enzymes involved in membrane-bound fatty acid elongation systems, were determined. The structure of the monkey *ELOVL4* gene is similar to the human *ELOVL4* gene (Table 2). These two genes share 97% homology in cDNA sequence and 98% similarity in predicted amino acid sequence. Although the function of the human *ELOVL4* gene still remains unclear, the monkey *ELOVL4* gene also conserves features typical of members of the *ELO* gene family (Fig. 2). In addition, remarkable expression of the *ELOVL4* gene was detected in the monkey retina (Fig. 3). These findings suggest that the monkey *ELOVL4* gene also has an important role in biosynthesis of VLCFA in the retina. The retina is known to have the ability to synthesize

fatty acid with carbon chain lengths up to 36 [22, 23], and this fact might be explained by the highly expressed *ELOVL4* gene. Furthermore, the *ELOVL4* gene in the retina was found to be expressed predominantly in cone and rod photoreceptor cells (Fig. 4). Based on the predicted function of ELOVL4 and its tissue and cellular localization, it could be hypothesized that ELOVL4 is associated with the biosynthesis of fatty acids, especially in photoreceptors, and play a crucial role in photoreceptor cell functions.

Real-time quantitative PCR also revealed that the monkey *ELOVL4* gene was expressed in the skin and thymus. This is the first report to indicate that the *ELOVL4* gene is expressed abundantly not only in the retina but also in the skin and thymus. The expression level in the brain, previously reported [5], was comparatively high among the other tissues, but was only about 9% of that in the retina. No significant expression was detected in the other tissue tested (Fig. 3). Tissue-restricted expression patterns have been reported for the *ELO2* and *ELO3* genes in rodents [10]. In rodents, the *ELO2* gene is reported to be expressed in the liver and testis, on the other hand, the expression of the *ELO3* gene is observed in the liver, skin and the brown fat of cold-exposed mice. These findings strongly suggest that different components of membrane-bound fatty acid elongation systems are involved in each tissue, and that the *ELOVL4* gene may have a particularly important role in the systems of brain, skin, thymus and retina.

It is reported that VLCFA are found at especially high levels in the brain and skin [24]. In the brain, sphingolipids, which contain VLCFA are considered to have an important role in the enhancement of electric insulation of myelin [25]. Sphingolipids are also believed to contribute unique structural properties to the epidermal water barrier in the skin [26]. Although the functional role of VLCFA and membrane-bound fatty acid elongation systems in the retina remains to be determined, growing evidence indicates that the lipid environment influences photoreceptor function [27–29]. This study does not give any insight into the function of the *ELOVL4* gene in the retina. However, the obtained information may be useful for evaluating the normal function of *ELOVL4* in the fatty acid chain elongation systems in the retina using non-human primates. Furthermore, the obtained gene sequence makes it possible to investigate the involvement of the *ELOVL4* gene in non-human primate macular degeneration.

The nucleotide sequence data reported in this paper have been submitted to GenBank and have been assigned the accession numbers AF461182, AF461183, AF461184, AF461185, AF461186 and AF461187.

References

1. Stone, E.M., Nichols, B.E., Kimura, A.E., Weingeist, T.A., Drack, A., and Sheffield, V.C. 1994. Clinical features of a Stargardt-like dominant progressive macular dystrophy with genetic linkage to chromosome 6q. *Arch. Ophthalmol.* 6: 765–772.
2. Edwards, A.O., Miedziak, A., Vrabec, T., Verhoeven, J., Acott, T.S., Weleber, R.G., and Donoso, L.A. 1999. Autosomal dominant Stargardt-like macular dystrophy: I. Clinical characterization, longitudinal follow-up, and evidence for a common ancestry in families linked to chromosome 6q14. *Am. J. Ophthalmol.* 4: 426–435.
3. Griesinger, I.B., Sieving, P.A., and Ayyagari, R. 2000. Autosomal dominant macular atrophy at 6q14 excludes CORD7 and MCDR1/PBCRA loci. *Invest. Ophthalmol. Vis. Sci.* 1: 248–255.
4. Lagali, P.S., MacDonald, I.M., Griesinger, I.B., Chambers, M.L., Ayyagari, R., and Wong, P.W. 2000. Autosomal dominant Stargardt-like macular dystrophy segregating in a large Canadian family. *Can. J. Ophthalmol.* 6: 315–324.
5. Zhang, K., Kniazeva, M., Han, M., Li, W., Yu, Z., Yang, Z., Li, Y., Metzker, M.L., Allikmets, R., Zack, D.J., Kakuk, L.E., Lagali, P.S., Wong, P.W., MacDonald, I.M., Sieving, P.A., Figueroa, D.J., Austin, C.P., Gould, R.J., Ayyagari, R., and Petrukhin, K. 2001. A 5-bp deletion in ELOVL4 is associated with two related forms of autosomal dominant macular dystrophy. *Nat. Genet.* 1: 89–93.
6. Bernstein, P.S., Tammur, J., Singh, N., Hutchinson, A., Dixon, M., Pappas, C.M., Zabriskie, N.A., Zhang, K., Petrukhin, K., Leppert, M., and Allikmets, R. 2001. Diverse Macular Dystrophy Phenotype Caused by a Novel Complex Mutation in the ELOVL4 Gene. *Invest. Ophthalmol. Vis. Sci.* 13: 3331–3336.
7. Oh, C.S., Toke, D.A., Mandala, S., and Martin, C.E. 1997. ELO2 and ELO3, homologues of the Saccharomyces cerevisiae ELO1 gene, function in fatty acid elongation and are required for sphingolipid formation. *J. Biol. Chem.* 28: 17376–17384.
8. Toke, D.A. and Martin, C.E. 1996. Isolation and characterization of a gene affecting fatty acid elongation in Saccharomyces cerevisiae. *J. Biol. Chem.* 31: 18413–18422.
9. Tvrdik, P., Asadi, A., Kozak, L.P., Nedergaard, J., Cannon, B., and Jacobsson, A. 1997. Cig30, a mouse member of a novel membrane protein gene family, is involved in the recruitment of brown adipose tissue. *J. Biol. Chem.* 50: 31738–31746.
10. Tvrdik, P., Westerberg, R., Silve, S., Asadi, A., Jakobsson,

A., Cannon, B., Loison, G., and Jacobsson, A. 2000. Role of a new mammalian gene family in the biosynthesis of very long chain fatty acids and sphingolipids. *J. Cell. Biol.* 3: 707–718.

11. El-Mofty, A., Gouras, P., Eisner, G., and Balazs, E.A. 1978. Macular degeneration in rhesus monkey (Macaca mulatta). *Exp. Eye. Res.* 4: 499–502.
12. Stafford, T.J., Anness, S.H., and Fine, B.S. 1984. Spontaneous degenerative maculopathy in the monkey. *Ophthalmology* 5: 513–521.
13. Ishibashi, T., Sorgente, N., Patterson, R., and Ryan, S.J. 1986. Pathogenesis of drusen in the primate. *Invest. Ophthalmol. Vis. Sci.* 2: 184–193.
14. Dawson, W.W., Ulshafer, R.J., Engel, H.M., Hope, G.M., and Kessler, M.J. 1989. Macular disease in related rhesus monkeys. *Doc. Ophthalmol.* 3: 253–263.
15. Monaco, W.A. and Wormington, C.M. 1990. The rhesus monkey as an animal model for age-related maculopathy. *Optom. Vis. Sci.* 7: 532–537.
16. Hope, G.M., Dawson, W.W., Engel, H.M., Ulshafer, R.J., Kessler, M.J., and Sherwood, M.B. 1992. A primate model for age related macular drusen. *Br. J. Ophthalmol.* 1: 11–16.
17. Nicolas, M.G., Fujiki, K., Murayama, K., Suzuki, M.T., Mineki, R., Hayakawa, M., Yoshikawa, Y., Cho, F., and Kanai, A. 1996. Studies on the mechanism of early onset macular degeneration in cynomolgus (Macaca fascicularis) monkeys. I. Abnormal concentrations of two proteins in the retina. *Exp. Eye. Res.* 3: 211–219.
18. Nicolas, M.G., Fujiki, K., Murayama, K., Suzuki, M.T., Shindo, N., Hotta, Y., Iwata, F., Fujimura, T., Yoshikawa, Y., Cho, F., and Kanai, A. 1996. Studies on the mechanism of early onset macular degeneration in cynomolgus monkeys. II. Suppression of metallothionein synthesis in the retina in oxidative stress. *Exp. Eye. Res.* 4: 399–408.
19. Shanklin, J., Whittle, E., and Fox, B.G. 1994. Eight histidine residues are catalytically essential in a membrane-associated iron enzyme, stearoyl-CoA desaturase, and are conserved in alkane hydroxylase and xylene monooxygenase. *Biochemistry* 43: 12787–12794.
20. Jackson, M.R., Nilsson, T., and Peterson, P.A. 1990. Identification of a consensus motif for retention of transmembrane proteins in the endoplasmic reticulum. *Embo J.* 10: 3153–3162.
21. Cinti, D.L., Cook, L., Nagi, M.N., and Suneja, S.K. 1992. The fatty acid chain elongation system of mammalian endoplasmic reticulum. *Prog. Lipid. Res.* 1: 1–51.
22. Aveldano, M.I. 1987. A novel group of very long chain polyenoic fatty acids in dipolyunsaturated phosphatidylcholines from vertebrate retina. *J. Biol. Chem.* 3: 1172–1179.
23. Rotstein, N.P. and Aveldano, M.I. 1988. Synthesis of very long chain (up to 36 carbon) tetra, penta and hexaenoic fatty acids in retina. *Biochem. J.* 1: 191–200.
24. Poulos, A. 1995. Very long chain fatty acids in higher animals—a review. *Lipids* 1: 1–14.
25. Bourre, J.M., Paturneau-Jouas, M.Y., Daudu, O.L., and Baumann, N.A. 1977. Lignoceric acid biosynthesis in the developing brain. Activities of mitochondrial acetyl-CoA-dependent synthesis and microsomal malonyl-CoA chain-elongating system in relation to myelination. Comparison between normal mouse and dysmyelinating mutants (quaking and jimpy). *Eur. J. Biochem.* 1: 41–47.
26. Wertz, P.W. 1992. Epidermal lipids. *Semin. Dermatol.* 2: 106–113.
27. Organisciak, D.T., Darrow, R.M., Jiang, Y.L., and Blanks, J.C. 1996. Retinal light damage in rats with altered levels of rod outer segment docosahexaenoate. *Invest. Ophthalmol. Vis. Sci.* 11: 2243–2257.
28. Weisinger, H.S., Vingrys, A.J., Bui, B.V., and Sinclair, A.J. 1999. Effects of dietary n-3 fatty acid deficiency and repletion in the guinea pig retina. *Invest. Ophthalmol. Vis. Sci.* 2: 327–338.
29. Mizota, A., Sato, E., Taniai, M., Adachi-Usami, E., and Nishikawa, M. 2001. Protective effects of dietary docosahexaenoic acid against kainate-induced retinal degeneration in rats. *Invest. Ophthalmol. Vis. Sci.* 1: 216–221.

Available online at www.sciencedirect.com
SCIENCE DIRECT®
Gene 318 (2003) 45–53
GENE
AN INTERNATIONAL JOURNAL ON GENES AND GENOMES
www.elsevier.com/locate/gene

Characterization of *AOC2* gene encoding a copper-binding amine oxidase expressed specifically in retina

Qiang Zhang[a,b], Yukihiko Mashima[b], Setsuko Noda[c], Yutaka Imamura[b], Jun Kudoh[d], Nobuyoshi Shimizu[d], Takatsune Nishiyama[a,b], Shinsuke Umeda[a,e], Yoshihisa Oguchi[b], Yasuhiko Tanaka[a], Takeshi Iwata[a,*]

[a] *National Institute of Sensory Organs, National Tokyo Medical Center, 2-5-1 Higashigaoka, Meguro, Tokyo 152-8902, Japan*
[b] *Department of Ophthalmology, Keio University School of Medicine, 35 Shinanomachi, Shinjuku, Tokyo 160-8582, Japan*
[c] *Department of Nursing, School of Health Sciences, Tokai University, Boseidai, Isehara, Kanagawa 259-1193, Japan*
[d] *Department of Molecular Biology, Keio University School of Medicine, 35 Shinanomachi, Shinjuku, Tokyo 160-8582, Japan*
[e] *Department of Biomedical Science, Graduate School of Agricultural and Life Sciences, The University of Tokyo, 1-1-1 Yayoi, Bunkyo, Tokyo 113-8657, Japan*

Received 15 March 2003; received in revised form 28 May 2003; accepted 13 June 2003

Received by S. Yokoyama

Abstract

We have previously cloned a human, retina-specific, amine oxidase gene (RAO, gene symbol: *AOC2*), a member of the copper-binding amine oxidase super family. *AOC2* shares sequence identity with the human kidney amine oxidase gene (KAO, gene symbol: *AOC1*) and the vascular adhesion protein-1 gene (VAP-1, gene symbol: *AOC3*). For further analysis of *AOC2*, the sequences surrounding the human *AOC2* and the complete mouse and partial rat homologue of *AOC2* were cloned for characterization. Real-time quantitative PCR, in situ hybridization, and immunohistochemistry were performed to determine the specific expression of *AOC2* in the mouse retina and especially in the retinal ganglion cells. Our results demonstrated that the copper-binding motif and the enzyme active site of *AOC1* and *AOC3* were both conserved in mouse *AOC2*. The human and mouse *AOC2* was flanked by two genes, the *Psme3* gene for PA-28 gamma subunit and, surprisingly, the *AOC3* gene. Rat *AOC2* contained a stop codon that terminated the peptide length to 127 amino acids. The presence of human and rat *AOC* pseudogene in this region, in addition to the tandemly positioned two *AOC* genes, indicates the possibility of successful *AOC3* replication to retina-specific *AOC2* for human and mouse but unsuccessful for rat.

Keywords: Amines; Copper amine oxidase; GABA; Oxidase; Retina; Retinal ganglion cells

1. Introduction

The amine oxidases are a group of enzymes that catalyze the conversion of biogenic amines to the corresponding aldehydes as shown in the following equation:

$$R^1CH_2NHR^2 + O_2 + H_2O \rightarrow R^1CHO + R^2NH_2 + H_2O_2.$$

The substituents, R^1 and R^2, determine the reactivity of various substrates by different amine oxidases (Houen, 1999). Four classes of amine oxidases are currently identified: monoamine oxidases (MAO) including MAO A and MAO B (Berry et al., 1994); polyamine oxidases (Hölttä, 1977); lysyl oxidases (Trackman et al., 1990); and copper-containing amine oxidases (Houen et al., 1993). Different amine oxidases have been identified in the eye (Fernandez de Arriba et al., 1991; Imamura et al., 1997).

The copper-containing amine oxidases are important regulators of cellular polyamine levels and are found in a wide range of species. They have broad substrate specificities, such as histamine, putrescine, spermine, and spermidine (Houen et al., 1993). In addition to the removal of polyamines and putrescine, copper-containing amine oxidases are involved in immune regulation, cellular growth

Abbreviations: PCR, polymerase chain reaction; RACE, rapid amplification of cDNA ends; bp, base pair; kb, kilobase.

* Corresponding author. Tel./fax: +81-3-34111026.
E-mail address: iwatatakeshi@kankakuki.go.jp (Y. Tanaka).

0378-1119/$ - see front matter © 2003 Elsevier B.V. All rights reserved.
doi:10.1016/S0378-1119(03)00753-4

regulation, differentiation, and apoptosis (Bachrach et al., 1987).

We have previously cloned a human, retina-specific amine oxidase (*AOC2*) gene located on chromosome 17q21 (Imamura et al., 1997, 1998). This gene encoded a novel protein that is a retina-specific amine oxidase (RAO). The amino acid sequence of *AOC2* shared a 38% identity with kidney amine oxidase (KAO, EC 1.4.3.6; Barbry et al., 1990), and had high homology with human kidney diamine oxidase (Barbry et al., 1990; Chassande et al., 1994). However, human *AOC2* showed the highest (65%) amino acid identity with vascular adhesion protein 1 (VAP-1, gene symbol: *AOC3*), which was initially cloned as human placental amine oxidase (Zhang and McIntire, 1996; Zhang et al., 1995).

AOC3 is an endothelial cell surface glycoprotein inducible under inflammatory conditions. *AOC3* functions as an amine oxidase with substrate benzylamine, but also participates in lymphocyte recirculation by mediating the binding of lymphocytes to peripheral lymph node endothelial cells (Smith et al., 1998; Bono et al., 1998a,b).

The purpose of this study was to further investigate *AOC2* by cloning and characterizing the mouse and rat homologue of *AOC2*. The results of detailed analysis of *AOC2* gene structure and the surrounding genes, which differed between species, are discussed. The trace of a possible insertion and deletion by DNA transposition in this region in mouse and rat are also discussed. A comparison of all three sequences of *AOC* (*AOC1*, *AOC2*, and *AOC3*) in three species is demonstrated for the first time.

2. Materials and methods

2.1. Isolation of mouse AOC2 gene and amplification of cDNA by RT-PCR and 5′/3′ RACE

Human *AOC2* cDNA (Imamura et al., 1997) was used as a probe to screen a mouse genomic phage library (Mouse 129/SvEvTacfBR Lambda Genomic Library, Stratagene, La Jolla, CA). Phage DNA was extracted from positive phage clones using a phage DNA isolation kit (Qiagen Lambda Mini Kit, Qiagen, Valencia, CA).

Mouse retinal cDNA was generated from the mRNA extracted from 129SVJ or ICR mice retinas with an mRNA extraction kit (MicroPoly(A) Pure Kit, Ambion, Austin, TX). Partial mouse *AOC2* cDNA was obtained by PCR amplification (SuperScript ONE-STEP RT-PCR System, Life Technologies, Rockville, MD) of mouse retina cDNA using primers, P1 (5′-CAGTGCCAGCCATGAATCTCA-3′) and P6 (5′-TCCTCTCTGCTCAGGACCTG-3′), which were designed to be within the identical sequence region of mouse and human *AOC2* genomic sequence.

The missing 5′ and 3′ cDNA sequence were obtained by the 5′/3′ RACE method (Marathon cDNA Amplification Kit, Clontech Laboratories, Palo Alto, CA) according to the manufacturer's instructions. Antisense primer, P4 (5′-GTAGCTCCAGCCCCACAGGGTGAAGGA-3′) and sense primer P3 (5′-CTGTCTTGAACTACAATGGCTC-3′) were used for 5′- and 3′-RACE, respectively, with adaptor-specific primer provided by the manufacturer (Fig. 3).

The cDNA and the genomic sequence were compared to determined gene structure of mouse *AOC2*. Sequencing reaction was performed by dideoxy terminator cycle sequencing kit (CEQ-2000XL DNA Analysis System, Beckman Coulter, Fullerton, CA).

2.2. Protein sequence analysis of AOC2 and AOC3

The membrane-spanning domain of *AOC2* and *AOC3* were predicted by TopPred II program (Clarosand von Heijne, 1994). Potential glycosylation sites were predicted by the program developed by Hansen et al. (1995).

2.3. Amplification of 5′ cDNA end and exon 1 of rat AOC2

Partial rat *AOC2* cDNA was amplified by RT-PCR (mRNA Selective PCR kit ver1.1, Takara, Japan) using primers, R1 (5′-CAGTGCCAGCCATGAATCTCA-3′) and R2 (5′-TCCTCTCTGCTCAGGACCTG-3′) designed to be within the identical sequence region of mouse and human *AOC2* cDNA sequences. Messenger RNA was extracted from rat (Sprague–Dawley) retinas with mRNA extraction kit (MicroPoly (A) Pure Kit, Ambion). The 5′ end of rat *AOC2* cDNA sequence was obtained by the 5′ RACE method (5′RACE System for Rapid Amplification of cDNA Ends Reagent Assembly ver 2.0, Life Technologies) according to the manufacturer's protocol. The primers used were: 5′-TCAGGAAAGCTGTGTT-3′, 5′-ATGTCCAGCATTGT-

Fig. 1. The mouse *AOC2* complete nucleotide sequence, deduced amino acid, potential glycosylation sites, and protein comparison with mouse *AOC3*. (A) The complete 2553-bp cDNA sequence of mouse *AOC2* encodes 757 amino acids. Numbers to the right refers to nucleotides and single capital letters under nucleotide sequence represents encoded amino acid. The first nucleotide of each exon is underlined and boldfaced. The polyadenylation signal (AATAAA) is indicated by (++++++). Predicted copper-binding motif and active site are also indicated as filled-in box. Location of primers used for PCR amplification of mouse *AOC2* probe for in situ hybridization (P2 and P5), cDNA amplification of mouse *AOC2* by RT-PCR method (P1 and P6), and 5′/3′-RACE methods (P3 and P4) are underlined. Potential N-glycosylation and O-glycosylation sites are indicated by open box and open circle, respectively. (B) Comparison of transmembrane domain (TMD with arrow) and potential glycosylation sites of mouse *AOC2* and *AOC3* are shown. The copper-binding motif (CBD with arrow), active sites (AS with arrow), O-glycosylation sites (O with filled arrow), and N-glycosylation sites (N with arrow) are indicated.

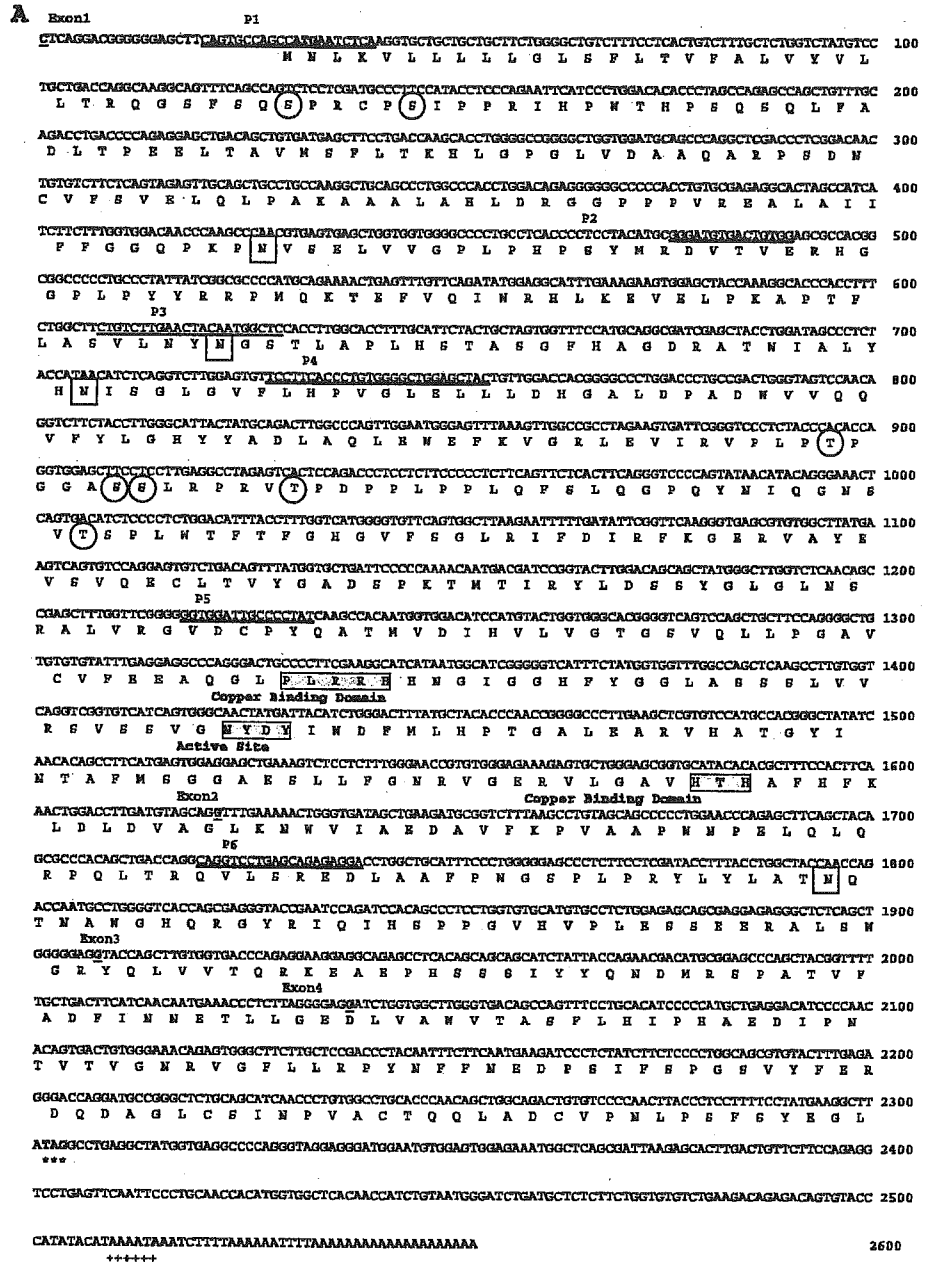
A
Exon1
P1
P2
P3
P4
P5
P6
Copper Binding Domain
Active Site
Exon2
Exon3
Exon4
B
RAO
VAP-1
NH2
COOH
TMD
CBD
AS
CBD
50 amino acids

CGCTTATGA-3′, and 5′-CACACTCACCCTTGAACC-GAATA-3′. The genomic fragment between exon 11 of rat *Psme3* gene for PA-28 gamma-subunit and rat *AOC2* exon 1 was amplified by PCR from rat genomic DNA (Sprague–Dawley) using sense primer designed from exon 11 of *Psme3* within the identical sequence region between mouse and human. The antisense primer was designed from the 5′ end of rat *AOC2* cDNA. Both cDNA and genomic sequences were compared to determine exon 1 of rat *AOC2*.

2.4. Cloning and sequencing of genomic DNA surrounding mouse and human AOC2

The homology of the DNA sequences between the *Psme3* and *AOC2* genes was determined by sequencing the PCR product generated between mouse *Psme3* exon 11 and *AOC2* exon 1. The sequence between mouse *AOC2* and *AOC3* was also determined by sequencing the PCR product generated between mouse *AOC2* exon 4 and *AOC3* exon 1.

Human BAC clone, KB551F9, isolated previously (Imamura et al., 1997), was sequenced by primers specific to human *AOC2* and *AOC3* cDNA sequences to determine the DNA sequence between the two genes with the Applied Biosystems 377 DNA sequencer using a PRISM DyeDeoxy Terminator cycle sequencing kit (PE Biosystems, Foster City, CA).

2.5. Measurements of AOC2 mRNA expression by real time quantitative PCR

Real-time quantitative PCR analysis of mouse *AOC2* transcript in retina, brain, heart, liver, lung, spleen, and testis was performed (GeneAmp® 5700 sequence detection system, PE Biosystems) (Higuchi et al., 1993). The PCR primer sets, 5′-TGCATACACACGCTTTCCACTT-3′ and 5′-TGTGGGCGCTGTAGCTGAAG-3′, were designed by Primer Express software (PE Biosystems). Five micrograms of total RNA extracted from each tissue were converted to cDNA by SuperScript preamplification system (Invitrogen, Tokyo, Japan). Amplified PCR products were detected by double-stranded DNA binding dye SYBR Green I (SYBR Green PCR master mix, PE Biosystems). The expression level was standardized with 18S ribosomal RNA gene as an internal control. Ribosomal 18S forward primer 5′-TTCGGAACTGAGGCCATGAT-3′ and reverse primers 5′-TTCGCTCTGGTCCGTCTTG-3′ were used for amplification. Expression level for each tissue was calculated based on a standard curve created using a template plasmid containing mouse *AOC2* cDNA according to the manufacturer's manual. To avoid detecting nonspecific PCR products, the purity of the PCR product was confirmed by agarose gel analysis and by melting curve analysis according to the manufacturer's manual.

2.6. In situ hybridization of AOC2 in mouse retina

Eyes excised from BALB/cA Jcl mice were rapidly embedded in OCT compound (Tissue-Tek, Sakura Finetechnical, Tokyo, Japan) and frozen in dry ice–ethanol solution. These tissue blocks were sectioned into 5-μm sections with a cryostat (Bright Instrument, Cambridgeshire, England) followed by air-drying on coated glass slides. Probes for in situ hybridization were amplified with primers fused with the T7 promoter sequence (Fig. 1). For antisense probe amplification, primer pair P2 (5′-GGGATGTGACTGTGG-3′) and 5′-TCAGTAATACGACTCACTATAGGGG-CAATCCACC-3′; and for sense probe amplification, primer pair 5′-AGCTTAATACGACTCACTATAGGGATGT-GACTGTGG-3′ and P5 (5′-ATAGGGGCAATCCACC-3′) were used. Amplified PCR products were purified by DNA purification kit (Wizard PCR Preps Purification System, Promega, Madison, WI). RNA probes were generated using DIG RNA labeling kit (Roche Molecular Biochemicals, Tokyo, Japan) according to the manufacturer's instructions. Sections were fixed in 4% paraformaldehyde in PBS and pretreated with proteinase K (Imamura et al., 1998). The hybridization cocktail contained 2 μg/ml RNA probe, 1 mg/ml *Escherichia coli* tRNA, 10 mM Tris–HCl, pH 8.0, 2.5 mM EDTA, pH 8.0, 1 × Denhardt's solution, 0.6 M NaCl, 50% deionized formamide, and 10% dextran sulfate. After 16 h of hybridization at 37 °C, the slides were washed twice in 60% formamide and 1 × SSC for 30 min at 42 °C, once in 2 × SSC for 30 min at 42 °C, and finally twice in 0.2 × SSC for 30 min each at 42 °C. Then, hybridization signals were detected with anti-DIG antibody conjugated with alkaline phosphatase and revealed by reaction with BCIP (5-bromo-4-chloro-3-indolylphosphate) and NBT (nitroblue tetrazoliumchloride) in the dark. The sense probe was used as control.

2.7. Immunohistochemical analysis of AOC2 in mouse retina

The distribution of *AOC2* in mouse retina was determined by immunohistochemical staining with antimouse *AOC2* peptide antibody. An antimouse *AOC2* peptide antibody was produced by immunizing rabbits with a peptide corresponding to residues 745–757 at the C-terminal of mouse *AOC2*. BALB/cA mice were euthanized by carbon dioxide, and the nucleated eyes were placed into 4% paraformaldehyde (PFA) in phosphate-buffered solution (PBS) for 10 h, embedded in paraffin, and cut into serial 5-μm sections.

Immunohistochemical staining was performed with the DAKO ENVISION System HRP Rabbit (DAKO, Carpinteria, USA) according to the manufacturer's instructions. Normal rabbit immunoglobulin was used for negative control. After deparaffinization and rehydration, sections were briefly digested with proteinase K before 10 min incubation in peroxidase. Sections were incubated with 2% skim milk

at room temperature for 30 min to block nonspecific binding, incubated at 4 °C for 16 h with the primary antibody, washed three times in PBS, then incubated at room temperature for 1 h with anti-rabbit HRP-conjugated secondary antibody before development with 3-amino-9-ethyl carbazole substrate.

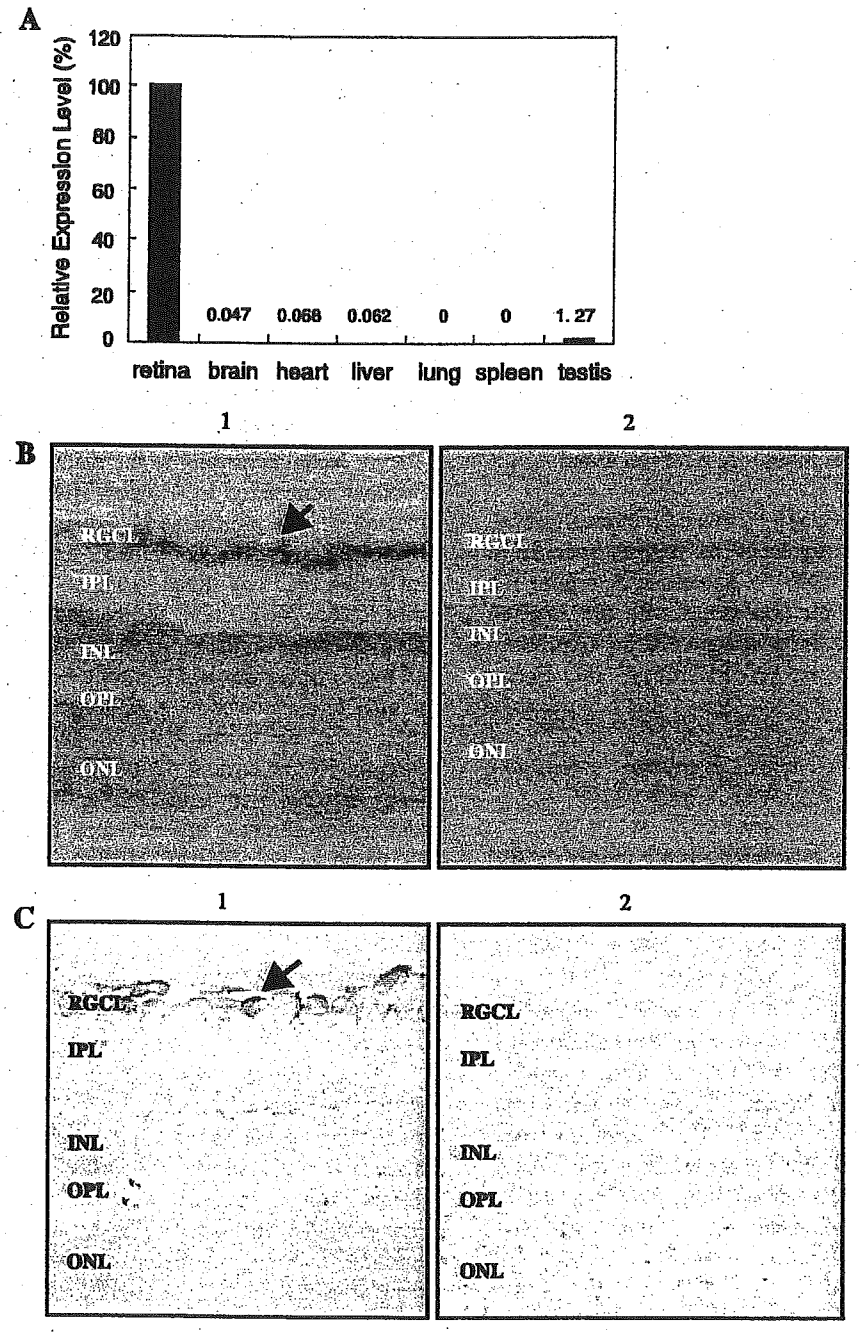

Fig. 2. Expression of *AOC2* in the mouse retina. (A) Real-time quantitative-PCR of mouse *AOC2* in retina, brain, heart, liver, lung, spleen, and testis was performed as described in Materials and methods. Expression levels of *AOC2* mRNA in each tissue are shown relative to expression in the retina as 100%. Numbers on the *x*-axis correspond to the relative expression level for each tissue. (B) In situ hybridization: Partial cDNA of mouse *AOC2* was amplified by PCR to generate templates for sense and antisense digoxigenin-labeled RNA probes, followed by in situ hybridization as described in Materials and methods. (1) In situ hybridization using antisense probe. The positive purple hybridization signal (arrow) was detected predominantly in retinal ganglion cell layer. (2) In situ hybridization using sense probe. No signal was detected by sense probe. (C) Immunostaining showed specific localization in retinal ganglion cell layer. Bar = 50 μm. (1) Immunostaining using antimouse *AOC2* antibody. Positive red staining was observed predominantly in retinal ganglion cell layer (arrow). (2) Immunostaining using normal immunoglobulin as negative control. No signal was detected. (IPL, inner plexiform layer; INL, inner nuclear layer; OPL, outer plexiform layer; and ONL, outer nuclear layer).

3. Results

3.1. Sequence analysis of mouse and rat AOC2

The complete mouse *AOC2* cDNA and gene were determined. The mouse *AOC2* cDNA (2553 bp) encodes the 757 amino acid, which is one amino acid longer than that of the human gene (Fig. 1A). The full-length cDNA sequence of mouse *AOC2* can be obtained from GenBank under accession number AF350445. The amino acid sequence identity between mouse *AOC2* and human *AOC1*, human *AOC2*, mouse *AOC3*, and human *AOC3* was 37%, 80%, 61%, and 60%, respectively. The copper-binding site and an active site conserved in *AOC1* and *AOC3* were also conserved in mouse *AOC2*. Unlike human *AOC2*, no splice variant was observed in the mouse *AOC2* gene (Imamura et al., 1998).

The TopPred II program used to predict the membrane-spanning domain of mouse *AOC3* between residues 6 and 16 at a score of 2.658 also predicted with confidence the same N-terminal region of *AOC2* between residues 5 and 17 at a score of 2.429 (Fig. 1B). Potential O- and N-glycosylation sites were predicted to be seven serine/threonine residues and four asparagine residues, respectively.

The 5′ end of rat *AOC2* exon 1 was cloned by 5′-RACE and PCR amplification of rat genomic DNA using primers designed to be between rat *Psme3* and rat *AOC2* exon 1. A stop codon was found approximately 400 bp downstream of the transcription start site, which shortened the theoretical peptide length to 127 amino acids.

3.2. Expression of AOC2 in mouse tissue

Real-time quantitative-PCR was performed on total RNA isolated from mouse retina, brain, heart, liver, lung, spleen, and testis to determine the relative expression level of *AOC2*. The absolute value of *AOC2* expression for each tissue was calculated based on the standard curve generated using plasmid-containing mouse *AOC2* cDNA. The absolute value for mouse retina, brain, heart, liver, lung, spleen, and testis were 3.23×10^{-5}, 2.16×10^{-8}, 2.28×10^{-8}, 2.72×10^{-8}, 0, 0, and 5.50×10^{-7} ng, respectively. *AOC2* expression was significantly higher in the retina than any of the other tissues (Fig. 2A). The second highest *AOC2* expression was observed in testis, which was only 1.27% of the retina.

In situ hybridization and immunostaining were performed to determine the transcript and translated product sites of *AOC2* in mouse retina. Specific hybridization of antisense probe was observed predominantly in the retinal ganglion cell layer (arrow, Fig. 2B-1), and weaker but recognizable signals were also observed in inner nuclear layer.

Immunostaining using antimouse *AOC2* peptide antibody showed specific localization of *AOC2* in retinal ganglion cells (arrow, Fig. 2C). No signal was detected when normal rabbit immunoglobulin was used as negative control.

3.3. Organization of mouse AOC2 and surrounding genes

The sequence analysis of *AOC2* and the surrounding regions revealed that *AOC2* was flanked by two different genes (Fig. 3). The *Psme3* gene for PA-28 gamma-subunit was located upstream of both mouse (GenBank accession number AB007139) and human *AOC2* (GenBank accession number XM_008202, AC055866). The distance between the mouse *Psme3* and *AOC2* was 1526 bp (Fig. 3).

AOC3 was found downstream of *AOC2* in both mouse (GenBank accession number AF078705) and human (GenBank accession number AB050500, NM_003734) genes. The distance between *AOC2* and *AOC3* in mouse and human were 775 and 478 bp, respectively (Fig. 3). The complete mouse *AOC2* gene sequence can be obtained from GenBank under accession number AF350446, and the sequence data of human *AOC3* and the promoter region has been deposited in GenBank under accession number AB050500, AB050501, and AB050502.

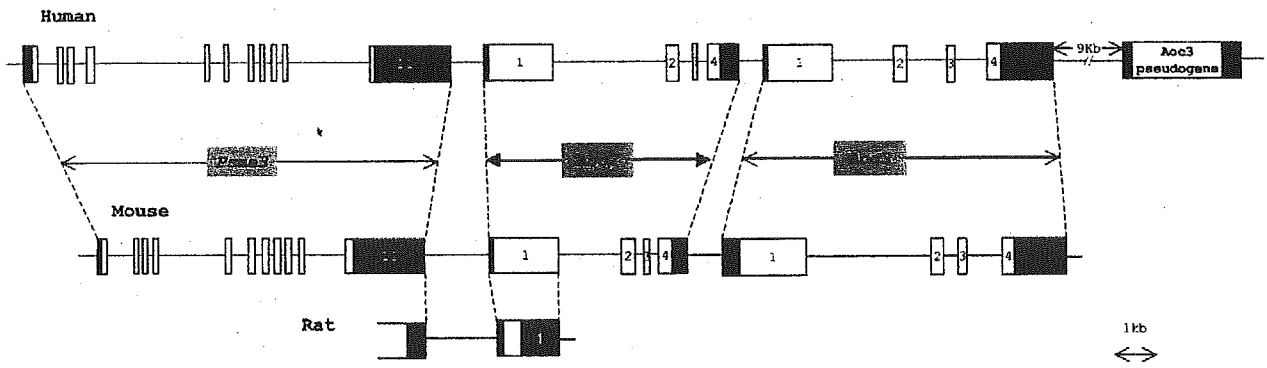

Fig. 3. Schematic diagram of human and mouse *AOC2* and the surrounding genes. The gene structure of *AOC2* and the surrounding genes were determined. Two genes, *Psme3* located upstream and *AOC3* located downstream of *AOC2*, were confirmed in both mouse and human. Exons of all three genes were positioned in the same direction. The open box indicates amino acid coding region and filled-in box indicate the noncoding region of the exon. Exon 1 of rat *AOC2* contained a stop codon that terminated the peptide length to 127 amino acids. Numbers in the box indicate exon numbers.

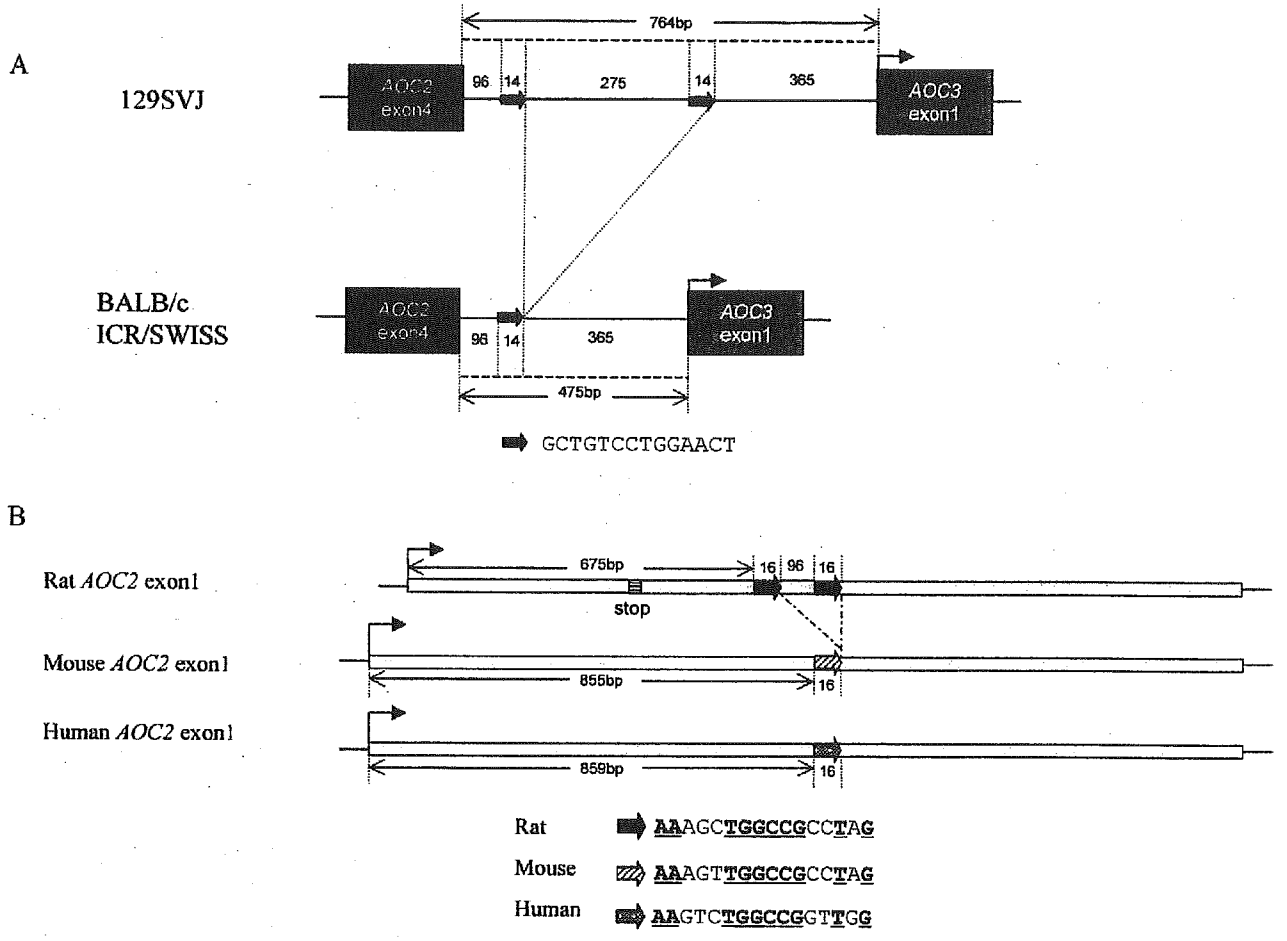

Fig. 4. DNA transposition in the promoter region of mouse *AOC3* and rat *AOC2* exon 1. (A) Additional sequences of 289 bp flanked by identical 14-bp sequence (5′-GCTGTCCTGGAACT-3′) was found in promoter region of *AOC3* in 129SVJ strain mouse, which was absent in BALB/c and ICR SWISS. (B) Insertion of 112 bp found in exon 1 of rat *AOC2* pseudogene. Inserted sequence is flanked by identical sequence of 16 bp, which is also found at the similar location in exon 1 of both mouse and human *AOC2*.

3.4. DNA transposition in mouse and rat AOC2

Several traces of DNA transposition were found in mouse and rat *AOC2*. Comparison of genomic sequences between three different strains of mice showed a 275 bp of nucleotide in 129SVJ mouse flanked by identical 14-bp sequence, 5′-GCTGTCCTGGAACT-3′, that was missing in BALB/c and ICR SWISS mice (Fig. 4A). Insertion of 96 bp in rat flanked by 16-bp sequence, 5′-AAAGCTGGCCGCC-TAG-3′, that was missing in mouse and human (Fig. 4B). In both cases, one of two short flanking sequences was present in the DNA without an insertion (Fig. 4A,B).

4. Discussion

Our results have confirmed the specific expression of mouse *AOC2* in the retina, and it was especially abundant in retinal ganglion cells. This is the first confirmation of the *AOC2* protein in retinal ganglion cells. This is significant because the retinal ganglion cells are the final retinal cells that process and deliver information to brain. Thus, any damage to retinal ganglion cells can directly influence the visual function of the eye.

Apoptosis of retinal ganglion cells is one of the major cause for blindness in patients with glaucoma, an optic neuropathy characterized by cupping of the optic disk and optic nerve degeneration, and is associated with scotomas in the visual field (Imamura et al., 1998).

We had suspected that the *AOC2* protein was involved in the production of γ-amino butyric acid (GABA) based on the previous reports of diamine oxidases (Seiler, 1980). However, our results suggest the possibility of an evolutionary link between *AOC2* and *AOC3*. Unexpectedly, we found that the 3′ end of the mouse *AOC2* genomic sequence in the 5′-flanking sequence of *AOC3* genomic sequence (GenBank accession number AF078705) (Bono et al., 1998a,b). This would suggest that *AOC2* and *AOC3* were

only separated by 775 bp (Fig. 3). This was later confirmed by the working draft of the mouse genome sequence containing *AOC2* and *AOC3* genes.

Human *AOC3*, previously discovered as a vascular adhesion protein, shares more than 65% of amino acid sequence with human *AOC2*, which is significantly higher than that of *AOC1* (38%). This is interesting as retina-specific amine oxidase was originally named after kidney amine oxidase. The copper-binding motif and active site (Mu et al., 1992, 1994) of *AOC1* are conserved in *AOC3* and has been confirmed to function as an amine oxidase when benzylamine was used as substrate. But its main function was recently described as an endothelial glycoprotein whose cell surface expression is significantly induced under inflammatory conditions.

AOC3 has been shown to participate in lymphocyte recirculation by mediating the binding of lymphocytes to peripheral lymph node endothelial cells in an L-selectin-independent fashion (Salmi and Jalkanen, 1992; Arvilommi et al., 1996). Expression of *AOC3* has been reported in various tissues including lung, appendix, small intestine, heart, placenta, skeletal muscle, ovary, lymph node, and several other tissues, while *AOC2* expression has been observed exclusively in the retina. A sequence comparison of mouse and human *AOC2* revealed several small but highly homologous regions in the proximal promoter region (data not shown). However, comparison of retina-specific mouse *AOC2* and non-tissue-specific *AOC3* promoter resulted in significantly lower sequence similarity, explaining the differences in expression profile of these two genes.

The two homologous genes, *AOC2* and *AOC3*, were tandemly located and had similar gene structure. This would suggest the possibility of a common ancestral gene. Tandem duplication of genes has been known to be a common mechanism to increase the members of a gene family and to generate new genes (Efstratiadis et al., 1980; Kawasaki et al., 1997).

Another amine-oxidase-like gene has been previously reported approximately 9-kb downstream of human *AOC3* (Cronin et al., 1998) (Fig. 3). This pseudogene lacked an intron, and the deduced amino acid sequence was similar to that of human *AOC3*/placental amine oxidase. The open reading frame was interrupted by in-frame stop codon, which restricted the amino acid length to 224. This amine-oxidase-like pseudogene was not found within 100-kb downstream of mouse *AOC3* when a search was made with CELERA mouse genome database (CELERA Discovery System, Gaithersburg, MD). When the cDNA and genomic sequence of rat *AOC2* were analyzed, to our surprise, exon 1 of rat *AOC2* contained a stop codon, which terminated the peptide length to only 17% of the mouse and human *AOC2*.

The discovery of a nonfunctional rat *AOC2* raises fundamental questions about its existence and the functional role of *AOC2*. One possible explanation is that *AOC2* can be replaced by *AOC3* or other amine oxidases that are also expressed in the rat retina. Undisrupted rat *AOC3* partial cDNA has been previously reported with high amino acid sequence identity of 95% and 83% to mouse and human, respectively (Morris et al., 1997). *AOC3* has been detected in the rat retina and may serve as a substitute for the missing *AOC2* in the rat retina.

These differences of gene organization and pseudogene location between species suggest that complex gene duplication has taken place in this region. We have found several traces of DNA transposition sites in the promoter region of mouse *AOC3* and in the exon 1 of rat *AOC2*. Both DNA insertions were non-long-terminal repeat (LTR) mobile element specific to this promoter confirmed by GenBank and CELERA Discovery System. Previously reported sequences contain disruption of active genes or activation on silent genes by various types of DNA transpositions (Plasterk, 1993; Smit, 1996).

The *AOC3* promoter of 129SVJ mouse 275 bp of DNA was inserted and flanked by identical sequence of 14 bp, which was not observed in BALB/c or ICR/SWISS mouse (Fig. 4A). Experiments designed to determine the effect of *AOC3* promoter by this DNA insertion would be of great interest. The 96-bp insertion found in exon 1 of the rat *AOC2*-like pseudogene was also flanked by identical 16-bp, which had no direct influence on the location of stop codon but potentially altered the coding frame. Similar sequence to this 16-bp flanking sequence was also found at the similar location in exon 1 of both mouse and human *AOC2* (Fig. 4B). If these short sequences found in mouse and human *AOC2* are equivalent to the flanking 16-bp sequence in rat *AOC2*-like pseudogene, functional *AOC2* might have evolved by this DNA insertion.

The copper-binding motif and active site of *AOC1* and *AOC3* are also conserved in *AOC2*. The TopPred II program (Claros and von Heijne, 1994) predicted a membrane-spanning domain at the N-terminal of mouse *AOC3* at residues 6 to 16 as previously reported but also predicted with confidence another at residues 5 to 17 at the same N-terminal region of *AOC2* (Fig. 1B). Glycosylation sites for *AOC2* were found at similar locations especially the N-terminal before the active site. All of our data predicted that *AOC2* had similar protein properties as *AOC3*, and because both genes are tandemly located, we propose the possibility that *AOC2* evolved evolutionarily from *AOC3* to become a retina-specific gene that encodes a novel adhesion protein. The adhesion molecular property of *AOC2* is now under investigation.

Acknowledgements

The authors thank M. Sasaki and M. Kobayashi for technical assistance. This work was supported in part by Grants-in-Aid for Research on Eye and Ear Sciences from Ministry of Health Labour and Welfare, Scientific Research (B) and Exploratory Research from the Ministry of Education, Science, Sports, and Culture of Japan; and Fund

for "Research for the Future" Program from the Japan Society for the Promotion of Science (JSPS).

References

Arvilommi, A.M., Salmi, M., Kalimo, K., Jalkanen, S., 1996. Lymphocyte binding to vascular endothelium in inflamed skin revisited: a central role for vascular adhesion protein-1 (*AOC3*). Eur. J. Immunol. 26, 825–833.

Bachrach, U., Ash, I., Abu-Elheiga, L., Hershkovitz, M., Loyter, A., 1987. Fusion-mediated microinjection of active amine and diamine oxidases into cultured cells: effect on protein and DNA synthesis in chick embryo fibroblasts and in glioma cells. J. Cell. Physiol. 131, 92–98.

Barbry, P., Champe, M., Chassande, O., Munemitsu, S., Champigny, G., Lingueglia, E., Maes, P., Frelin, C., Tartar, A., Ullrich, A., et al., 1990. Human kidney amiloride-binding protein: cDNA structure and functional expression. Proc. Natl. Acad. Sci. U. S. A. 87, 7347–7351.

Berry, M.D., Juorio, A.V., Paterson, I.A., 1994. The functional role of monoamine oxidases A and B in the mammalian central nervous system. Prog. Neurobiol. 42, 375–391.

Bono, P., Salmi, M., Smith, D.J., Jalkanen, S., 1998a. Cloning and characterization of mouse vascular adhesion protein-1 reveals a novel molecule with enzymatic activity. J. Immunol. 160, 5563–5571.

Bono, P., Salmi, M., Smith, D.J., Leppanen, I., Horelli-Kuitunen, N., Palotie, A., Jalkanen, S., 1998b. Isolation, structural characterization, and chromosomal mapping of the mouse vascular adhesion protein-1 gene and promoter. J. Immunol. 161, 2953–2960.

Chassande, O., Renard, S., Barbry, P., Lazdunski, M., 1994. The human gene for diamine oxidase, an amiloride binding protein. Molecular cloning, sequencing, and characterization of the promoter. J. Biol. Chem. 269, 14484–14489.

Claros, M.G., von Heijne, G., 1994. TopPred II: an improved software for membrane protein structure predictions. Comput. Appl. Biosci. 10, 685–686.

Cronin, C.N., Zhang, X., Thompson, D.A., McIntire, W.S., 1998. cDNA cloning of two splice variants of a human copper-containing monoamine oxidase pseudogene containing a dimeric *Alu* repeat sequence. Gene 220, 71–76.

Efstratiadis, A., Posakony, J.W., Maniatis, T., Lawn, R.M., O'Connell, C., Spritz, R.A., DeRiel, J.K., Forget, B.G., Weissman, S.M., Slightom, J.L., Blechl, A.E., Smithies, O., Baralle, F.E., Shoulders, C.C., Proudfoot, N.J., 1980. The structure and evolution of the human beta-globin gene family. Cell 21, 653–668.

Fernandez de Arriba, A., Lizcano, J.M., Balsa, D., Unzeta, M., 1991. Contribution of different amine oxidases to the metabolism of dopamine in bovine retina. Biochem. Pharmacol. 42, 2355–2361.

Hansen, J.E., Lund, O., Engelbrecht, J., Bohr, H., Nielsen, J.O., Hansen, J.E., 1995. Prediction of O-glycosylation of mammalian proteins: specificity patterns of UDP-GalNAc:polypeptide N-acetylgalactosaminyltransferase. Biochem. J. 308, 801–813.

Higuchi, R., Fockler, C., Dollinger, G., Watson, T., 1993. Kinetic PCR: real time monitoring of DNA amplification reactions. Biotechnology 11, 1026–1030.

Houen, G., 1999. Mammalian Cu-containing amine oxidases (CAOs): new methods of analysis, structural relationships, and possible functions. APMIS. Acta Pathol. Microbiol. Immunol. Scand., Suppl. 96 (107), 5–46.

Houen, G., Jorgensen, J., Leonardsen, L., Larsson, L.I., 1993. Purification and partial characterization of mammalian Cu-dependent amine oxidases. Acta Chem. Scand. 47, 902–909.

Hölttä, E., 1977. Oxidation of spermidine and spermine in rat liver: purification and properties of polyamine oxidase. Biochemistry 16, 91–100.

Imamura, Y., Kubota, R., Wang, Y., Asakawa, S., Kudoh, J., Mashima, Y., Oguchi, Y., Shimizu, N., 1997. Human retina-specific amine oxidase (*AOC2*): cDNA cloning, tissue expression, and chromosomal mapping. Genomics 40, 277–283.

Imamura, Y., Noda, S., Mashima, Y., Kudoh, J., Oguchi, Y., Shimizu, N., 1998. Human retina-specific amine oxidase: genomic structure of the gene (*AOC2*), alternatively spliced variant, and mRNA expression in retina. Genomics 51, 293–298.

Kawasaki, K., Minoshima, S., Nakato, E., Shibuya, K., Shintani, A., Schmeits, J.L., Wang, J., Shimizu, N., 1997. One-megabase sequence analysis of the human immunoglobulin lambda gene locus. Genome Res. 7, 250–261.

Morris, N.J., Ducret, A., Aebersold, R., Ross, S.A., Keller, S.R., Lienhard, G.E., 1997. Membrane amine oxidase cloning and identification as a major protein in the adipocyte plasma membrane. J. Biol. Chem. 272, 9388–9392.

Mu, D., Janes, S.M., Smith, A.J., Brown, D.E., Dookey, D.M., Klinman, J.P., 1992. Tyrosine codon corresponds to topa quinone at the active site of copper amine oxidases. J. Biol. Chem. 267, 7979–7982.

Mu, D., Medzihradszky, K.F., Adams, G.W., Mayer, P., Hines, W.M., Burlingame, A.L., Smith, A.J., Cai, D., Klinman, J.P., 1994. Primary structures for a mammalian cellular and serum copper amine oxidase. J. Biol. Chem. 269, 9926–9932.

Plasterk, R.A., 1993. Molecular mechanisms of transposition and its control. Cell 74, 781–786.

Salmi, M., Jalkanen, S., 1992. A 90-kilodalton endothelial cell molecule mediating lymphocyte binding in humans. Science 257, 1407–1409.

Seiler, N., 1980. On the role of GABA in vertebrate polyamine metabolism. Physiol. Chem. Phys. 12, 411–429.

Smit, A.F.A., 1996. The origin of interspersed repeats in the human genome. Curr. Opin. Genet. Dev. 6, 743–748.

Smith, D.J., Salmi, M., Bono, P., Hellman, J., Leu, T., Jalkanen, S., 1998. Cloning of vascular adhesion protein 1 reveals a novel multifunctional adhesion molecule. J. Exp. Med. 188, 17–27.

Trackman, P.C., Pratt, A.M., Wolanski, A., Tang, S.S., Offner, G.D., Troxler, R.F., Kagan, H.M., 1990. Cloning of rat aorta lysyl oxidase cDNA: complete codons and predicted amino acid sequence. Biochemistry 29, 4863–4870.

Zhang, X., McIntire, W.S., 1996. Cloning and sequencing of a copper-containing, topa quinone-containing monoamine oxidase from human placenta. Gene 179, 279–286.

Zhang, X., Kim, J., McIntire, W.S., 1995. cDNA sequences of variant forms of human placenta diamine oxidase. Biochem. Genet. 33, 261–268.

Original Paper

Ophthalmic Research

Ophthalmic Res 2003;35:345–350
DOI: 10.1159/000074075

Received: April 29, 2002
Accepted after revision: September 16, 2003

Variants of the Myocilin Gene in Japanese Patients with Normal-Tension Glaucoma

Kanako Izumi[a,b] Yukihiko Mashima[b] Minoru Obazawa[a] Yuichiro Ohtake[b] Tomihiko Tanino[b] Hiroshi Miyata[b] Qiang Zhang[b] Yoshihisa Oguchi[b] Yasuhiko Tanaka[a] Takeshi Iwata[a]

[a]National Tokyo Medical Center, National Institute of Sensory Organs, Meguro-ku, and
[b]Department of Ophthalmology, Keio University School of Medicine, Shinjuku-ku, Japan

Key Words
Myocilin · Polymorphism · Normal-tension glaucoma · Primary open-angle glaucoma · Gene expression · COS-1 cell

Abstract
Myocilin *(MYOC)* mutations are associated with juvenile- and adult-onset primary open-angle glaucoma (POAG). The purpose of this study was to determine whether *MYOC* gene mutations are associated with normal-tension glaucoma (NTG). The prevalence of *MYOC* mutations was determined in 80 Japanese NTG patients and 100 control subjects. In addition, the expression of mutant *MYOC* was determined by transforming COS-1 cells with five myocilin variants (R158Q, D208E, I360N, A363T, and I477S) and examining whether myocilin was present in the cultured cells and/or the culture medium by western blotting. Six different nucleotide sequence variants, R46Stop, R76K, R158Q, D208E, A488A, and one in the 3′ non-coding region, were identified in 80 NTG patients. The differences in the frequencies of these sequence changes in NTG patients did not differ significantly from those in 100 control Japanese subjects. COS-1 cells transfected with the wild type, R158Q, or D208E variants secreted myocilin into the culture medium. On the other hand, the detected myocilin was significantly reduced in the medium of cells transfected with the I360N, A363T, or I477S variants that were previously identified as mutations for POAG. Definitive evidence of *MYOC* variants associated with NTG was not found.

Introduction

Primary open-angle glaucoma (POAG) is an important cause of blindness worldwide. The disease is characterized by visual-field changes corresponding to the excavation of the optic disk and is usually associated with an elevation of the intraocular pressure (IOP). Although the pathogenesis of glaucomatous optic neuropathy is poorly understood, it is generally accepted that the IOP is a major risk factor. In eyes with normal-tension glaucoma (NTG), there is no evidence for an increase in the IOP over 21 mm Hg at any time. It has been suggested that vascular insufficiencies are deeply involved in the development and progression of NTG [1–3].

KARGER
Fax +41 61 306 12 34
E-Mail karger@karger.ch
www.karger.com

0030–3747/03/0356–0345$19.50/0

Accessible online at:
www.karger.com/ore

Takeshi Iwata
National Tokyo Medical Center
National Institute of Sensory Organs
2-5-1 Higashigaoka, Meguro, Tokyo 152-8902 (Japan)
Tel./Fax +81 3 34111026, E-Mail iwatatakeshi@kankakuki.go.jp

There is strong evidence that genetic factors play a role in the pathogenesis of glaucoma, and several chromosomal loci involved with POAG have been identified. The first of these loci, the trabecular meshwork inducible glucocorticoid response (TIGR), was shown to be the product of the glaucoma gene, *GLC1A,* which was mapped to chromosome 1q [4]. At the time of that report, we cloned a novel protein in the photoreceptors of the retina that had some sequence homology to non-muscle myosin and olfactomedin, and called this protein myocilin [5]. This protein was later found to be identical to TIGR. The *GLC1A* gene is now known as the myocilin *(MYOC)* gene. Mutations in the *MYOC* gene have been more commonly associated with juvenile-onset POAG (36% of patients with this disease) [6] than with adult-onset POAG [6–8] (3–5% with adult onset). The role of myocilin and the mechanism through which the mutations in this gene cause glaucoma remains unknown. Approximately 50 mutations in the *MYOC* gene have been described that probably cause glaucoma [6–10].

Myocilin, a 57-kD protein, is encoded by a gene with three exons and is 504 amino acids in length [11]. The third exon of the *MYOC* gene encodes a peptide sequence that is homologous to olfactomedin, and the vast majority of *MYOC* mutations in patients with POAG have been identified in the olfactomedin homology domain [6–10]. On the other hand, some mutations in the *MYOC* gene have been reported to be associated with NTG patients [9, 12, 13], although Clark et al. [14] have suggested that coding sequence variations in the *MYOC* gene were not commonly involved in NTG.

In Japan, the prevalence of glaucoma is approximately 3.5% in patients over 40 years old, and the incidence of POAG is 0.58% and of NTG 2.04% [15]. The prevalence of NTG in the Japanese population is high compared with that in other populations. We have evaluated the potential pathogenicity of mutations of the *MYOC* gene in patients with NTG in two ways. First, we compared the prevalence of mutations in the *MYOC* gene in NTG patients and in control subjects. And second, we determined the expression of mutant *MYOC* by transforming these mutants into COS-1 cells and measuring the amount of myocilin in the medium or in the cell. These experiments were performed based on the report that normal myocilin is secreted from cultured cells, but very little or no myocilin is secreted from cells expressing the mutant forms of myocilin associated with POAG [16].

Materials and Methods

Patients

Blood samples were collected from 80 unrelated NTG patients regardless of their family history at the Keio University Hospital. All subjects signed an informed consent after an explanation of the procedures to be used and the purpose of the studies.

All of the NTG patients were diagnosed by two glaucoma specialists (Y.O. and T.T.) according to the following criteria: presence of typical optic disk damage with glaucomatous cupping and loss of the neuroretinal rim; reproducible visual field defect compatible with glaucomatous cupping; untreated peak IOP that was ≤21 mm Hg at all times, including both the 5 baseline measurements and the diurnal testing (every 3 h from 6.00 to 24.00 h); open drainage angles on gonioscopy, and the absence of any secondary cause for glaucomatous optic neuropathy, such as a previously raised IOP following trauma, or a period of steroid administration or uveitis. The demographic features of 80 NTG patients were: 44 men and 36 women, mean age at the initial diagnosis was 54.0 ± 12.8 years, mean highest diurnal IOP was 16.3 ± 2.8 mm Hg (range 11–21), and the mean values of the mean deviation (MD) and corrected pattern standard deviation (CPSD) on Humphrey perimetry (program 30-2) were −7.59 ± 6.98 dB and −6.52 ± 4.87 dB, respectively.

Control blood samples were obtained from 100 Japanese individuals who had an IOP below 20 mm Hg, had no glaucomatous disk changes, and no family history of glaucoma.

Mutation Screening of the MYOC *Gene*

Genomic DNA was prepared by proteinase K-phenol-chloroform extraction. The methods used to detect mutations in the *MYOC* gene have been described [9]. Mutations in the *MYOC* gene were first screened for by PCR-SSCP analysis using a standard protocol with specific primers. Samples with abnormal mobility were further analyzed by direct sequencing of the PCR products with an automated DNA sequencer (373A, Applied Biosystems, Foster City, Calif., USA) using a Thermo Sequenase Dye Terminator Cycle Sequencing kit (Amersham Pharmacia Biotech, Piscataway, N.J., USA).

Myocilin Constructs

Human *MYOC* cDNA was obtained by RT-PCR amplification (Super Script One Step RT-PCR System, Invitrogen Japan, Tokyo, Japan) of cDNA generated from total RNA isolated from human trabecular meshwork cells. Human *MYOC* cDNA was cloned into vector pcDNA3.1(+) (Invitrogen), and the following variants were generated with the Quick Change Multi Site-Directed Mutagenesis Kit (Stratagene, La Jolla, Calif., USA): R158Q (present study), D208E (present study), I360N (pathologic mutant for POAG [9]), A363T (pathologic mutant for POAG [9]), and I477S (pathologic mutant for POAG [16, 17]) according to the manufacturer's instructions. The sense-strand primer sequences used for mutagenesis (underlined letters) were:

R158Q:
5′-GGAGGAAGAGAAGAAGC<u>A</u>ACTAAGGCAAGAAAATG-3′

D208E:
5′-CGTGGAATTTGGA<u>G</u>ACTTTGGCCTTCCAGG-3′

I360N:
5′-GGCTGAGAAGGAAA<u>A</u>CCCTGGAGCTGGCTA-3′

A363T:
5′-GGAAATCCCTGGA<u>A</u>CTGGCTACCACGGACA-3′

I477S:
5′-AAGTACAGCAGCATGA<u>G</u>TGACTACAACCCCCTG-3′

R76Lys has already been reported as a polymorphism worldwide. The clinical phenotype of R46Stop is not consistent with the genotype, and this mutation may not be associated with glaucoma [18]. Thus, we did not examine these two sequence variations for the expression of myocilin.

Cell Culture, Myocilin Transfection, and Sample Preparation

COS-1 cells were grown in Dulbecco's modified Eagle's medium (DMEM) with 10% fetal bovine serum (FBS) and antibiotics. For transient transfection, COS-1 cells were harvested from 175 cm^2 flasks (Falcon 3111) by trypsinization, pelleted by centrifugation, and washed twice in 10 ml phosphate buffered saline (PBS, pH 7.4), and resuspended in PBS at a concentration of 1×10^7 cells/ml. Ten micrograms of plasmid DNA (pcDNA3.1(+)) were added to 500 µl of COS-1 cells and electroporated in a 0.4-cm cuvette with a Gene Pulser II Electroporator (Nippon BioRad Laboratories, Yokohama, Japan) set at 500 V, 100 µF. Electroporated cells were resuspended in 2 ml of medium and plated into 75 cm^2 flasks (Falcon 3108) at a concentration of 5.0×10^7 cells. The medium was changed after 24 h. Serum-free medium was added 12 h prior to cell and medium collection. The cells were harvested after 60 h. Five milliliters of serum-free medium was concentrated by centrifugation in a Centricon 50 spin column (Millipore, Bedford, Mass., USA) to achieve a 100-fold concentration. Samples were stored at –80 °C.

The transformed COS-1 cells were rinsed with PBS and cellular proteins were extracted in 2.4 ml of mammalian protein extraction buffer (M-PER, Pierce, Rockford, Ill., USA) containing 0.4 ml of protease inhibitors (Complete EDTA-free Protease Inhibitor Cocktail, Roche Diagnostics Japan, Tokyo, Japan). The cell extract was centrifuged at 3,000 rpm for 5 min, and the supernatant was stored at –80 °C. The protein concentration was determined with the Coomassie Protein Assay Reagent (Pierce).

RNA Isolation and RT-PCR

Total RNA was isolated from cultured COS-1 cells with a total RNA isolation kit (RNA-Bee-RNA Isolation Reagent; TEL-Test, Friendswood, Tex., USA). Total RNA samples were digested by RNase-free DNase (Roche Diagnostics, Japan) to minimize the risk of genomic DNA contamination. First-strand cDNA was synthesized using random primers (Super Script First-Strand Synthesis System for RT-PCR; Invitrogen Japan).

PCR was performed using 1 µg of single-strand cDNA with 2.5 U *Taq* DNA polymerase in a volume of 50 µl. After predenaturation at 95 °C for 5 min, 25 cycles were performed including denaturation at 95 °C for 30 s, annealing at 65 °C for 30 s, and extension at 72 °C for 1 min, followed by 1% agarose gel electrophoresis. The primers used were: 5′-ACACAGGCACAGGTATCAGCAAGA-3′ (sense primer) and 5′-AAGTTGTCCCAGGCAAAGAGCTT-3′ (antisense primer). Ribosomal RNA 18S was examined as a control. The primers used were: 5′-TTCGGAACTGAGGCCATGAT-3′ (sense primer) and 5′-TTCGCTCTGGTCCGTCTTG-3′ (antisense primer).

SDS-PAGE and Western Blot

SDS-PAGE and Western immunoblotting of transfected COS-1 cells were performed. Fifteen-microliter samples of COS-1 medium or cell extract were applied to 12% polyacrylamide gels. Proteins were transferred to Protran BA85 Cellulosenitrat (Schleicher & Schuell, Dassel, Relliehausen, Germany), blocked for 1 h with the blocking solution containing 10% Milk Diluent/Blocking Solution (KPL, Gaithersburg, Md., USA) and 0.1% Tween-20 in phosphate buffer saline (pH 7.4). The membrane was probed with a rabbit polyclonal antihuman myocilin peptide antibody 4381R (1 µg/ml). This anti-human myocilin antibody was generated against peptide sequence TRDTARAVPPGSREVST corresponding to positions between amino acid 188 and 204. The peptide antibody was initially described by Karali et al. [■■■]. The specific signal was detected by incubation of antirabbit IgG HRP secondary antibody (New England BioLabs, Beverly, Mass., USA) followed by a chemiluminescence reaction with Luminol reagent A and peroxide reagent B as recommended by the manufacturer (New England BioLabs) and made visible with chemiluminescence imager (Lumi-Imager F1, Roche Applied Science, Tokyo, Japan).

Antibody specificity was confirmed by absorbance of antibody by antigen peptide before Western blotting (fig. 2c). Antibody (10 µg) was absorbed with 1,000-fold molar ratio of purified antigen peptide (TRDTARAVPPGSREVST) for 1 h at room temperature in 10 ml of blocking solution before incubation with the blot. The absorbed antibody was tested by Western blotting against secreted wild-type myocilin mixture. Further experimental conditions were the same as described above.

Results

Screening of MYOC *in NTG Patients*

We identified six different sequence variations of *MYOC* in the patients with NTG (table 1). Variants in codon 46 (R46Stop), codon 158 (R158Q), and codon 488 (A488A) were not found in the 100 normal controls. The frequency of other sequence changes (R76K, D208E, and 3′ non-coding) in NTG patients did not differ significantly from the frequencies in the control subjects.

Expression of MYOC mRNA in COS-1 Cells

No differences in the *MYOC* transcripts were found between the wild type and variants as compared with those of ribosomal 18S mRNA as an internal standard (fig. 1).

Expression of Myocilin in COS-1 Cells and Medium

Myocilin was expressed in COS-1 cells transformed by wild-type *MYOC*, or by R158Q and D208E variants (fig. 2a, lanes 1–3). A significant lower expression of myocilin was observed in cells transformed with variants I360N, A363T, and I477S (fig. 2a, lanes 4–6). Myocilin was secreted into the medium of COS-1 cells that were transfected by the wild-type *MYOC*, and by R158Q, or D208E variants (fig. 2b). On the other hand, the secreted myocilin was significantly lower in the medium of COS-1 cells that were transfected by variants I360N, A363T, and I477S.